Open access • Journal Article • DOI:10.1680/GEOT.11.P.052

Dynamic Winkler modulus for axially loaded piles — Source link

George Anoyatis, George Mylonakis

Institutions: University of Patras

Published on: 01 Jun 2012 - Geotechnique (Thomas Telford Ltd)

Topics: Pile, Soil structure interaction and Displacement field

Dynamic Winkler modulus for axially-loaded piles

George Anoyatis
Department of Civil Engineering, University of Patras, Rio, Greece, GR-26500

George Mylonakis (Corresponding author)
Department of Civil Engineering, University of Patras, Rio, Greece, GR-26500
Phone: +30-2610-996542, Fax: +30-2610-996576, e-mail: mylo@upatras.gr

Abstract

The problem of axial dynamic pile-soil interaction and its analytical representation using the concept of a dynamic Winkler support are revisited. It is shown that depth- and frequency-dependent Winkler springs and dashpots, obtained by dividing the complex-valued side friction and the corresponding displacements along the pile, may faithfully describe the interaction effect, contrary to the common perception that the Winkler concept is always approximate. An axisymmetric wave solution, based on linear elastodynamic theory, is then derived for the harmonic steady-state response of finite and infinitely-long piles in a homogeneous viscoelastic soil stratum, with the former type of piles resting on rigid rock. The pile is modelled as a continuum, without the restrictions associated with strength-of-materials approximations. Closed-form solutions are obtained for: (i) the displacement field in the soil and the pile; (ii) the stiffness and damping ("impedance") coefficients at the pile head; (iii) the actual, depth-dependent, dynamic Winkler moduli; (iv) a set of fictitious, depth-independent, Winkler moduli to match the dynamic response at the pile head. Results are presented in terms of dimensionless graphs, tables, and simple equations that provide insight into the complex physics of the problem. The predictions of the model compare favourably with existing solutions, while new results and simple design-oriented formulas are presented.

Notation

a_0	dimensionless frequency
$a_{res,m}$	m^{th} resonance of pile-soil system
$a_{cutoff} = a_{res,1}$	cutoff frequency or first resonance of pile-soil system
A_p	pile cross-sectional area
A, B, C, D	integration constants
d	pile diameter
G_p, E_p	pile shear modulus, pile Young's modulus
G_s, E_s	soil shear modulus, soil Young's modulus
$F(z)$	body force along pile axis
$k^*, k^*(z)$	complex-valued Winkler moduli
k	average (depth-independent) Winkler modulus
$k(z)$	depth-dependent Winkler modulus
K^*	complex-valued pile head stiffness
K_{st}, K	static and dynamic pile head stiffness
$K_0(), K_1(), I_0(), I_1()$	modified Bessel functions of zero and first order, and first and second kind
L	pile length, soil thickness
P	amplitude of pile head load
r	radial coordinate
u_r, u_θ, u_z	radial, tangential, vertical soil displacement
V_s, V_s^{pile}	shear wave propagation velocity in soil and pile material
w	vertical pile displacement
z	vertical coordinate

Greek symbols

α, α_m	positive variables
β	average (depth-independent) Winkler damping coefficient

$\beta(z)$	depth-dependent damping coefficient
β_p, β_s	pile, soil material damping
β_r	radiation damping coefficient
γ	Euler's number ($\simeq$0.577)
ζ	overall damping at the pile head
η_s, η_p	compressibility coefficient for soil and pile
λ	complex-valued Winkler wavenumber
λ_s, λ_p	wavelengths in soil and pile material, respectively
ν_p, ν_s	pile and soil Poisson's ratio
τ_{rz}^{pile}, τ_{rz}	pile and soil vertical shear stress
σ_z	soil vertical normal stress
ω	cyclic excitation frequency

Keywords: Dynamics, Elasticity, Piles, Soil/structure interaction, Theoretical Analysis, Vibration

Introduction

Modelling of dynamic pile-soil interaction has received significant research attention over the past four decades. Most studies are either purely numerical in nature (Blaney *et al*., 1976; Roesset, 1980; Syngros, 2004), or employ mixed analytical-numerical formulations of various degrees of sophistication (Kaynia & Kausel, 1982; Sanchez-Salinero, 1982; Banerjee & Sen, 1987; Rajapakse, 1990; Wolf *et al.*, 1992; Ji & Pak, 1996, Seo *et al.*, 2009). Other contributions focus on experimental aspects of the problem, both in the field (Blaney *et al*., 1987; Tazoh *et al*., 1987; El-Marsafawi *et al*., 1992) and the laboratory (Boulanger *et al*., 1999; Bhattacharya *et al.*, 2004; Knappett & Madabhushi, 2009). Purely analytical studies are based primarily on two-dimensional idealizations for wave propagation in the soil, associated with the approximate model of Baranov and Novak (Baranov, 1967; Novak, 1974; Novak *et al.*, 1978; Veletsos & Dotson, 1986; Mylonakis, 1995; El Naggar, 2000). On the other hand, analytical solutions based on three-dimensional wave propagation theory, which can provide more realistic predictions and shed light into fundamental aspects of dynamic pile-soil interaction, have been explored to a lesser degree (Tajimi, 1969; Nogami & Novak, 1976; Akiyoshi, 1982; Mylonakis, 2001b; Saitoh, 2005; Anoyatis, 2009).

With reference to simple engineering approximations, the most efficient way of modelling dynamic pile-soil interaction is to replace the soil medium by a series of independent Winkler springs and dashpots uniformly distributed along the pile axis. The substitution is convenient as the multi-dimensional boundary value problem is reduced to that of a simple rod subjected to one-dimensional wave propagation in the vertical direction. Although idealized, Winkler models are widely accepted by engineers, used for both axially and laterally-loaded piles under static or dynamic conditions (Novak, 1974; Randolph & Wroth, 1978; O'Rourke & Dobry, 1978; Baguelin & Frank, 1979; Scott, 1981; Pender, 1993; Guo, 2000; Reese & Van Impe, 2000). Their popularity stems primarily from their ability to (Mylonakis, 2001a): (1) yield realistic predictions of pile response, (2) incorporate variable soil properties with depth and radial distance from the pile, (3) model group effects by employing pertinent pile-to-pile

interaction models, (5) require substantially smaller computational effort than more rigorous alternatives.

The fundamental problem in the implementation of Winkler models lies in the assessment of the moduli of the Winkler springs and dashpots. Current methods for determining these parameters can be classified into three main groups (Mylonakis, 2001a): (A) experimental methods, (B) calibration with rigorous numerical solutions, (C) simplified theoretical models. Notwithstanding the significance of the above methods, they can all be criticized for certain drawbacks. For instance, experimentally-determined Winkler values pertain mostly to large-amplitude static loads and do not properly account for low-strain soil stiffness, energy dissipation and frequency effects (Novak, 1991; Reese & Van Impe, 2000). On the other hand, calibrations with rigorous numerical solutions in Group B may encounter numerical difficulties in certain parameter ranges, as for instance in the case of long compressible piles, resonant frequencies and regions in the vicinity of the pile head and tip. Also, these approaches are often limited by analytical and computational complexities associated with the underlying numerical procedures, which can make them unappealing to geotechnical engineers. Finally, plane-strain models in Group C are unstable at low frequencies (thereby unable to predict static settlements), cannot capture resonant frequencies and associated cutoff effects, require empirical adjustments and do not account for important factors such as the continuity of the medium in the vertical direction and the stiffness contrast between pile and soil (Randolph & Wroth, 1978; Baguelin & Frank, 1979; Novak, 1991; Mylonakis, 2001b).

With reference to methods in Group C, it appears that a rational model capable of providing improved estimates of dynamic Winkler stiffness and damping to be used in engineering applications would be desirable. In the framework of linear elastodynamic theory, an approximate yet realistic analytical solution is presented in this paper for an axially-loaded pile in a homogeneous soil stratum. While maintaining conceptual and analytical simplicity, the proposed model has distinct advantages over other models in Group C: it is stable at low frequencies, accounts for resonant phenomena and cutoff frequency effects, encompasses the

continuity of the medium in the vertical direction and the compressibility of the soil material, and is free of empirical constants. Apart from its intrinsic theoretical interest, the study provides simplified expressions for static and dynamic Winkler moduli which can be used in engineering practice.

Problem Definition & Model Development

The problem considered in this article is depicted in Fig. 1: a vertical solid cylindrical pile embedded in a homogeneous soil medium, subjected to an axial harmonic head load of amplitude P and cyclic frequency ω, applied at the pile head. The soil is modelled as a continuum, resisting dynamic pile displacements through combined inertial forces and compression-shearing in the vertical direction. Soil is assumed to be a linear viscoelastic material of Young's modulus E_s, Poisson's ratio ν_s mass density ρ_s and linear hysteretic damping β_s expressed through the complex shear modulus $G_s^* = G_s(1+2i\beta_s)$. Unlike most previous studies, (e.g., Nogami & Novak, 1976; Akiyoshi, 1982), the pile is modelled as a continuum, without the limitations associated with strength-of-materials approximations. The pile is described by its diameter d, Young's modulus E_p, Poisson's ratio ν_p and mass density ρ_p . Both infinitely-long piles in a half-space and end-bearing piles of finite length L, resting on rigid rock, are considered. Perfect contact (i.e., no gap or slippage) is assumed at the pile-soil interface. Positive notation for stresses and displacements is depicted in Fig. 1.

With reference to the cylindrical coordinate system in Fig. 1, the equilibrium of an arbitrary soil element in the vertical direction is described by the differential equation

$$\frac{\partial(\tau_{rz}\, r)}{\partial r} + r\frac{\partial \sigma_z}{\partial z} + r\,\rho_s \frac{\partial^2 u_z}{\partial t^2} = 0 \qquad (1)$$

where τ_{rz} = shear stress on rz plane, σ_z = vertical normal stress, ρ_s = soil mass density, $u_z = u_z(r, z, t)$ = vertical soil displacement.

Fundamental to the analysis presented herein is the assumption that normal stress, σ_z, and shear stress, τ_{rz}, are controlled exclusively by the vertical displacement component u_z; the influence of radial displacement, u_z, on these stresses is considered negligibly small (Mylonakis, 2001a). Based on this physically motivated simplification, the stress-displacement relations for σ_z and τ_{rz} are written as

$$\sigma_z \simeq -\eta_s^2 G_s^* \frac{\partial u_z}{\partial z} \tag{2}$$

$$\tau_{rz} \simeq -G_s^* \frac{\partial u_z}{\partial r} \tag{3}$$

where G_s^* is the complex soil shear modulus and η_s a dimensionless compression parameter that depends solely on Poisson's ratio. The above approximation is attractive, as it leads to a straightforward uncoupling of the governing equations, unlike the case of the classical equations of elastodynamics (Graff, 1975). The negative sign in the right–hand side of these expressions conforms to the notation for stresses and displacements in Fig. 1. To satisfy the above requirements, zero radial stress, σ_r, in the soil may be assumed, as discussed in the ensuing.

Equations (2) and (3) were apparently first employed by Nogami & Novak (1976) for the analysis of the axial dynamic pile-soil interaction problem. In that work, however, the pile was modelled as a rod and the radial displacement of the medium was assumed to be zero. In the present study the assumptions would be less restrictive: u_z is not constant over the pile cross section and u_r is small but not zero; the influence of the latter displacement component in vertical equilibrium is incorporated into coefficient η_s. In this study,

$$\eta_s = \sqrt{\frac{2}{1-\nu_s}} \tag{4}$$

which conforms to the assumption $\varepsilon_\theta = 0$, $\sigma_r = 0$ that accounts, approximately, for the partial lateral restraint of the soil medium in axisymmetric deformation. This approach was followed by Mylonakis (2001a) for the analysis of the corresponding static problem and is extended here to the dynamic regime. The assumption of Nogami & Novak (1976), $\eta_s = \sqrt{2(1-\nu_s)/(1-2\nu_s)}$, is not adopted here as it leads to a stiffer medium and breaks down in the incompressible case ($\nu_s = 0.5$).

Considering forced harmonic oscillations of the type $u_z(r,z,t) = u_z(r,z)\exp(i\omega t)$, the equilibrium equation (1) can be expressed in the displacement form

$$\frac{\partial^2 u_z}{\partial r^2} + \frac{1}{r}\frac{\partial u_z}{\partial r} + \eta_s^2 \frac{\partial^2 u_z}{\partial z^2} + \left(\frac{\omega}{V_s^*}\right)^2 u_z = 0 \qquad (5)$$

where ω is the cyclic oscillation frequency and V_s^* the complex-valued propagation velocity of shear waves in the soil. Note that if the variation with depth of vertical normal stress $\partial\sigma_z/\partial z$ is neglected, the above formula simplifies to

$$\frac{\partial^2 u_z}{\partial r^2} + \frac{1}{r}\frac{\partial u_z}{\partial r} + \left(\frac{\omega}{V_s^*}\right)^2 u_z = 0 \qquad (6)$$

which expresses the cylindrical wave equation of the dynamic plane strain–model (Novak, 1974; Novak *et al.*, 1978). Setting $\omega = 0$ in the above expression yields the conventional static plane-strain model of Randolph & Wroth (1978) and Baguelin & Frank (1979), the solution of which requires introduction of an empirically-determined radius along which soil displacement is set equal to zero, to ensure finite displacements in the domain. In the same spirit, Novak (1991) considers an empirical minimum frequency in equation (6), to avoid the breakdown of the solution at low frequencies. Equation (5) is free of these drawbacks.

Introducing separation of variables, equation (5) yields the general solution

$$u_z = [A\, I_0(qr) + B\, K_0(qr)]\, (C \sin \alpha z + D \cos \alpha z) \tag{7}$$

where $I_0(), K_0()$ are the modified Bessel functions of zero order and first and second kind, respectively, and α is a positive real variable of dimensions 1/Length. A, B, C and D are integration constants to be determined from the boundary conditions. Variable q is related to α through the frequency-dependent equation

$$q = \sqrt{(\alpha \eta_s)^2 - \left(\frac{\omega}{V_s^*}\right)^2} \tag{8}$$

Note that in the special case $\omega = 0$ and $q = \alpha \eta_s$ the above expression reduces to the static solution of Mylonakis (2001a).

To ensure bounded response at large radial distances from the pile and satisfy the boundary condition of zero normal stress at the soil surface, constants A and C in equation (7) must vanish. Accordingly, the solution reduces to

$$u_z(r, z) = B\, K_0(q\, r)\, \cos \alpha z \tag{9}$$

in which constant D has merged into constant B.

Infinitely-long pile

Based on the properties of the Fourier transform, the response of the soil medium is obtained by integrating equations (3) and (9) over the positive variable α

$$u_z(r, z, \omega) = \int_0^\infty B\, K_0(q\, r)\, \cos \alpha z\, \, d\alpha \tag{10}$$

$$\tau_{rz}(r,z,\omega) = G_s^* \int_0^\infty B\, q\, K_1(q\, r)\, \cos\alpha z\, d\alpha \tag{11}$$

The corresponding equilibrium equation for the pile is

$$\frac{\partial^2 w}{\partial r^2} + \frac{1}{r}\frac{\partial w}{\partial r} + \eta_p^2 \frac{\partial^2 w}{\partial z^2} + \left(\frac{\omega}{V_s^{pile}}\right)^2 w = -\frac{F(z)}{G_p A_p} \tag{12}$$

in which $w = w(r,z,t)$ is the vertical pile displacement (which varies within a horizontal cross section) and V_s^{pile} is the propagation velocity of shear waves in the pile material. η_p is a dimensionless compressibility parameter analogous to that in equation (4). In this study,

$$\eta_p = \sqrt{2(1+\nu_p)} \tag{13}$$

which corresponds to the assumption $\sigma_r = \sigma_\theta = 0$. This approach is more realistic over equation (4) for the pile material, due to pile–soil stiffness contrast. It must be noticed that this assumption (like the one in equation (4)) does not satisfy the continuity of the medium in the radial direction. Accordingly, the model can be viewed as semi-continuum, since continuity is satisfied only in the vertical direction, as u_r is unspecified. Nevertheless, this violation is of minor importance from a practical viewpoint. The present analysis naturally leads to a solution that differs from the one obtained from the classical strength-of-materials modelling involving a rod with a stiffness of E_pA_p.

In equation (12), $F(z)$ stands for the body forces distributed along the pile. These can be determined by resolving the force P acting at the pile head into equivalent distributed loads in form of co-sinusoidal components

$$F(z) = \int_0^\infty \frac{2P}{\pi} \cos \alpha z \, d\alpha \tag{14}$$

in which parameter α is interpreted the same way as in equations (7) to (11).

Introducing separation of variables and enforcing the boundary conditions of zero normal stress at the pile head ($z=0$) and bounded displacements at the pile centreline ($r=0$), the following expressions for pile displacement and shear stress are obtained

$$w(r, z, \omega) = \int_0^\infty \left[C \, I_0(q_p \, r) + \frac{2P}{G_p \, A_p \, L \, q_p^2} \right] \cos \alpha z \; d\alpha \tag{15}$$

and

$$\tau_{rz}^{pile}(r, z, \omega) = - G_p \int_0^\infty C \, q_p \, I_1(q_p \, r) \cos \alpha z \; d\alpha \tag{16}$$

where C is an integration constant to be determined from the boundary conditions. In full analogy with the analysis of the soil material, q_p is connected to α through

$$q_p = \sqrt{(\alpha \eta_p)^2 - \left(\frac{\omega}{V_s^{pile}} \right)^2} \tag{17}$$

Imposing the continuity conditions (equations (10)-(11) and (15)-(16)) for stresses and displacements at the pile-soil interface, constants B and C can be determined as solutions to an algebraic system of two equations in two unknowns. This yields the solution for pile displacement

$$w(r,z,\omega) = \frac{2P}{G_p \pi^2} \int_0^\infty \frac{1}{s_p^2} \left[1 - \frac{I_0(q_p r)}{I_0(s_p)} \frac{X_2 K_1(s)}{K_0(s) X_1 + X_2 K_1(s)} \right] \cos \alpha z \, d\alpha \qquad (18)$$

which is valid in the region $0 \leq r \leq d/2$. In the above equation

$$X_1 = s_p^2, \qquad X_2 = \frac{G_s^*}{G_p} \frac{I_0(s_p)}{I_1(s_p)} s s_p \qquad (19)(19a,b)$$

are dimensionless complex parameters with $s = q\,d/2$ and $s_p = q_p\,d/2$, q and q_b given by equations (8) and (17), respectively. Note that material damping in the pile can be incorporated into the above solution by replacing G_p and V_s^{pile} by their complex counterparts $G_p^* = G_p(1+2i\beta_p)$ and $V_s^{pile\,*} = V_s^{pile}\sqrt{1+2i\beta_p}$.

End-bearing pile

For a pile of finite length resting on a rigid stratum, one must consider the additional restriction of vanishing soil and pile displacements at the base of the soil layer. Enforcing this condition equation (9) yields the discrete values

$$\alpha = \alpha_m = \frac{\pi}{2L}(2m-1), \qquad m = 1, 2, 3, \ldots \qquad (20)$$

which correspond to the solution of the eigenvalue problem $\cos(\alpha L) = 0$. Under this restriction, equations (8) and (17) are rewritten in the discrete form

$$q_m = \sqrt{(\alpha_m \eta_s)^2 - \left(\frac{\omega}{V_s^*}\right)^2} \quad , \quad q_{pm} = \sqrt{(\alpha_m \eta_p)^2 - \left(\frac{\omega}{V_s^{pile}}\right)^2} \qquad (21)(21a,b)$$

In the same spirit as before, the head force P can be resolved into co-sinusoidal components as

$$F(z) = \sum_{m=1}^{\infty} \frac{2P}{L} \cos \alpha_m z \tag{22}$$

The solution for the end-bearing pile is obtained by replacing the integrals in equations (10), (11), (15) and (18) with corresponding infinite sums involving parameters α_m, q_m, q_{p_m}; this yields the expression

$$w(r, z, \omega) = \frac{2P}{G_p \pi L} \sum_{m=1}^{\infty} \frac{1}{s_{p_m}^2} \left[1 - \frac{I_0(q_{p_m} r)}{I_0(s_{p_m})} \frac{X_{2m} K_1(s_m)}{K_0(s_m) X_{1m} + X_{2m} K_1(s_m)} \right] \cos \alpha_m z \tag{23}$$

where X_{1m}, X_{2m}, s_m, and s_{p_m} are modified parameters obtained from equations (19a,b) with $\alpha = \alpha_m$, $q = q_m$, and $q_p = q_{p_m}$. It is noted in passing that the classical strength-of-materials solution based on the assumption that pile cross sections remain plane, is obtained from equation (23) by setting $r = d/2$ and

$$X_{1m} = \alpha_m^2 - \frac{\omega^2 \tilde{m}_p}{E_p A_p} \quad , \quad X_{2m} = \frac{2 \pi s_m G_s^*}{E_p A_p} \tag{24}(24a,b)$$

where $\tilde{m}_p (= \rho_p A_p)$ is the pile mass per unit length. This substitution is also valid for infinitely-long piles.

In the ensuing and except where specifically otherwise indicated, the Fourier integrals are evaluated using dimensionless (αd) values varying between 10^3 and 10^4; corresponding infinite series are evaluated using 10^3 terms; ν_p, ν_s and β_p are taken equal to 0.25, 0.4 and 0, respectively. Pile settlement is evaluated at the pile periphery ($r = d/2$). As will be shown in

the ensuing, for stiff piles $(E_p/E_s \geq 100)$, this estimate deviates from settlement at the pile centreline $(r=0)$ by less than 1%.

Model Validation

Table 1 compares results for static stiffness of end-bearing piles obtained from the proposed model and from available solutions in the literature. The results are presented in terms of normalized static pile head stiffness $K_{st}/E_s\,d$. The performance of the model is satisfactory with mean and maximum deviations over the rigorous numerical solution by Kaynia & Kausel (1982) not exceeding approximately 3.5% and 8.5%, respectively.

In Figure 2 additional results for static stiffness of end-bearing piles are compared to available numerical approaches including rigorous finite–element and boundary–element solutions. It is seen that for soft piles $(E_p/E_s=100)$ the numerical results exhibit considerable scattering due to the sensitivity of the analyses to the discretisation of the pile. For instance, when a small number of elements are used (Poulos & Davis, 1980), an increase in stiffness with increasing pile length is observed in some of the solutions for $L/d>50$ – obviously an erroneous trend for end-bearing piles. In contrast, the present solution exhibits a stable behaviour and agrees well with the most rigorous results by El–Sharnouby & Novak (1990). Similar good agreement is observed for higher E_p/E_s ratios.

In the dynamic regime, pile head stiffness may be represented by a complex-valued impedance coefficient K^* which can be cast in the following equivalent forms

$$K^* = \mathrm{Re}(K^*) + i\,\mathrm{Im}(K^*) = K(\omega)(1+2i\zeta) \tag{25}$$

where $K(\omega)=\mathrm{Re}(K^*)$ is the storage stiffness and $2\zeta K(\omega)=\mathrm{Im}(K^*)$ is the loss stiffness. Dimensionless parameter $\zeta=\mathrm{Im}(K^*)/2\mathrm{Re}(K^*)$ is the equivalent damping ratio. K can be interpreted as a spring and $(2\zeta K/\omega)$ as a dashpot attached parallel to the spring at the pile head.

A set of comparisons against results from the rigorous numerical solution of Kaynia & Kausel (1982) is presented in Fig. 3, referring to dynamic pile impedance normalized by the static value K_{st} versus dimensionless frequency $a_0 = \omega d/V_s$. The accord between the proposed model and the numerical solution is satisfactory over the whole range of frequencies examined. Evidently, the influence of frequency on normalized pile head stiffness becomes more pronounced with soft and/or long piles. Also, an increase in frequency beyond a certain value leads to a sudden increase in damping due to the emergence of propagating waves in the medium. This threshold frequency corresponds to the fundamental resonant frequency of the soil medium in compression–extension (cutoff frequency) and is associated with a minimum stiffness value $K(\omega)$.

For stiff piles $(E_p/E_s = 1000)$, stiffness K appears insensitive to frequency as the ratio K/K_{st} varies between 1.05 and 0.93. Similarly, damping is less than 0.3 in the range $0 \leq a_0 \leq 1$. These patterns can be understood given that the vertical response of the system is governed mainly by the compliance of the pile rather than the soil. For soft piles $(E_p/E_s = 100)$, the variation in stiffness with frequency is stronger and damping is higher – an anticipated trend since the compliance of the system is controlled mainly by the soil medium. Evidently, the increase in damping is stronger for long piles and becomes less significant with decreasing slenderness ratio L/d.

The variation of vertical displacement within the pile cross section is depicted in Fig. 4 for two end-bearing piles. Despite the low pile-soil stiffness contrast $(E_p/E_s = 100)$, the variation between pile head settlement at the centreline and the periphery is less than five parts in a thousand for all cases examined. Analogous differences are observed at the mid-length of the pile.

Evaluation of Winkler Modulus

For an infinitely-long pile, the complex Winkler modulus k^* can be readily obtained by dividing the vertical soil reaction per unit pile length (dynamic side friction) with the corresponding pile settlement at the pile-soil interface i.e.,

$$k^*(z,\omega) = 2\pi G_s^* \frac{\int_0^\infty \frac{s\ K_1(s)\ \cos\alpha z}{K_0(s)\,X_1 + X_2\,K_1(s)}\ d\alpha}{\int_0^\infty \frac{K_0(s)\ \cos\alpha z}{K_0(s)\,X_1 + X_2\,K_1(s)}\ d\alpha} \tag{26}$$

where the dimensionless parameters X_1 and X_2 are given by equations (19a,b). For an end-bearing pile the corresponding equation is

$$k^*(z,\omega) = 2\pi G_s^* \frac{\sum_{m=1}^{\infty} \frac{s_m\ K_1(s_m)\ \cos\alpha_m z}{K_0(s_m)\,X_{1m} + X_{2m}\,K_1(s_m)}}{\sum_{m=1}^{\infty} \frac{K_0(s_m)\ \cos\alpha_m z}{K_0(s_m)\,X_{1m} + X_{2m}\,K_1(s_m)}} \tag{27}$$

The above ratios faithfully describe the variation of shear tractions ("side friction") along the pile, contrary to the common perception that the Winkler model is always approximate. Note that since Winkler constants are typically employed in conjunction with a rod model for the pile, some deviation in the results of the present analysis and a Winkler model is expected, when X_1 and X_2 are used based on equations (19a,b). Identical response will be obtained when X_1 and X_2 are based on equations (24a,b). The complex-valued Winkler modulus for both end-bearing and infinitely-long piles can be expressed, as before, in the typical form $k^* = k(1 + 2i\beta)$, k being the dynamic stiffness per unit pile length and β the corresponding damping coefficient. Note that the latter parameter encompasses both material (β_s) and radiation (β_r) damping in the soil (i.e., $\beta = \beta_s + \beta_r$).

With reference to an infinitely long pile, the variation of Winkler modulus with depth is presented in Fig. 5 for different frequencies, pile-soil stiffness ratios and soil material damping. For static conditions ($a_0 = 0$), a decreasing trend with depth is observed in all curves; for small E_p/E_s ratios the decrease is, naturally, more rapid. In the dynamic regime Winkler modulus exhibits undulations with frequency and depth. This is more pronounced for soft piles and low material damping (Fig. 5(a)). An increase in either material damping or pile-soil stiffness ratio suppresses the oscillatory behaviour. For stiff piles (Figs 5(b) and 5(d)) a distinct trend is observed: an increase in frequency generally leads to higher values of $k(z)$ which vary between $1-2.7\,G_s$, over the whole range of depths examined $(0-50\,d)$. For high values of material damping (Fig. 5(d)), the variation of k is restricted in the range $1-2\,G_s$.

Similar trends are observed for the damping coefficient β in Fig. 6. At zero frequency $(\omega = 0)$, β varies weakly with depth and is practically equal to soil material damping β_s. For stiff piles (Figs 6(b) and (d)), an increase in damping with frequency is evident combined with a weak variation with depth. For soft piles (Figs 6(a) and 6(c)) the variation with frequency is stronger. The singularity $(\beta \to \infty)$ observed in some of the curves is attributed to a zero k value at a certain depth. Accordingly, this effect does not suggest infinite loss of energy at the specific point, but merely a 90-degree phase difference between side resistance and pile displacement.

Additional results are provided in Figs 7 to 9 referring to end-bearing piles. Pile displacement, soil reaction and associated Winkler modulus (ratio of soil reaction to pile displacement) are plotted as functions of depth. Static behaviour is examined in Fig. 7 for different E_p/E_s and L/d ratios. High values of pile slenderness lead to faster attenuation of both pile displacement and soil reaction with depth. The trend is, understandably, more pronounced for soft piles ($E_p/E_s = 100$, Figs 7(a) and 7(b)). For short piles $(L/d = 10)$, displacements tend to attenuate almost linearly with depth, which suggests a column-like behaviour. On the other hand, for long piles linearity is lost and displacements die out exponentially. For very long piles $(L/d = 100)$ a strong gradient (boundary layer) in tractions and displacements is observed near the pile head, which is noticeable up to approximately the mid–depth of the profile. On the other hand, for

very short piles $(L/d=10)$ the whole pile length contributes to attenuation of displacement and side friction. In all cases, peak soil reactions and displacements always occur at the pile head and become zero at the tip. Their ratio (modulus k), however, is always finite at the tip.

The boundary layer phenomenon observed at $z=0$ can be understood in light of the requirement for maximum soil reaction near the pile head (to resist the applied load), and zero soil reaction (to satisfy the boundary condition of the traction-free surface). Evidently, soil reaction has to jump from zero to maximum over an infinitesimal distance, generating this pattern (Pak & Ji, 1993; Syngros, 2004).

With reference to Winkler modulus (Figs 7(c) and 7(f)), a decreasing trend with depth is observed in all curves. For short piles, $k(z)$ is always larger than in more slender piles of the same E_p/E_s ratio. The effect of pile-soil stiffness contrast on $k(z)$ is stronger in long piles: for $L/d=100$ and $E_p/E_s=100$, $k(z)$ varies between $0.2-2.8\,G_s$; for $E_p/E_s = 1000$, $k(z)$ varies between $1.1 - 2\,G_s$. On the other hand, for short piles, $k(z)$ depends solely on slenderness ratio; for $L/d=10$ it varies between $2.5-4.5\,G_s$ regardless of E_p/E_s.

Figures 8 and 9 present corresponding results in the dynamic regime. It is observed that displacements tend to attenuate faster with increasing frequency. This is anticipated given the increasing contribution of pile and soil inertia with frequency, which amplifies soil reaction and increases phase angle between excitation and response. The effect is understandably more pronounced in soft (Fig. 8(a)) than in stiff piles (Fig. 9(a)). Soil reactions tend to attenuate faster with depth than pile displacements – an anticipated trend in light of the properties of the Boussinesq point load solution. [Recall to this end that for a point load P acting at the surface of a halfspace stresses attenuate in proportion to z^{-2}, whereas displacements attenuate in proportion to z^{-1}]. This is naturally more pronounced in soft piles (Figs 8(b) and 9(b)). Dynamic soil resistance is more sensitive to frequency than displacements, exhibiting a slower attenuation with depth with increasing a_0. The variation with depth of dynamic spring (Figs 8(c) and 9(c)) and dashpot (Figs 8(f) and 9(f)) values resembles that of an infinitely-long

pile. For stiff piles, $k(z)$ varies between $1.6-2.8\,G_s$ over the whole pile length and the range of frequencies examined (Fig. 8(c)). For soft piles the variation is stronger, ranging from $0.8-3.2\,G_s$ (Fig. 9(c)).

The undulations in the attenuation of dynamic Winkler modulus with depth observed in Figs 8(c) and 9(c) can be understood in light of the wavelengths of the vertically propagating compressional waves in the pile and the soil. These are given in normalized form by the expressions

$$\lambda_s/d = \frac{2\pi}{a_0}\eta_s \tag{28}$$

$$\lambda_p/d = \frac{2\pi}{a_0}\eta_p \sqrt{\frac{1+\nu_s}{1+\nu_p}\,\frac{\rho_s}{\rho_p}\,\frac{E_p}{E_s}} \tag{29}$$

referring to the soil and the pile, respectively. These functions are plotted in Fig. 10 together with numerical data extracted from Figs 8(c) and 9(c). The observed wavelengths in pile response are associated with waves propagating in the soil rather than the pile material.

Average Dynamic Winkler Modulus

Given the complexities associated with the variation of Winkler modulus with depth, it is convenient to adopt a fictitious, depth-independent modulus, to be used in engineering calculations. This is achieved by equating the dynamic displacement at the pile head obtained from the proposed theory to that obtained from a Winkler approach (Mylonakis, 2001a). Although this naturally introduces some error in the analysis (especially regarding the distribution of internal stresses in the pile), it is desirable as it greatly simplifies the solution.

Assuming k^* to be constant within a homogeneous layer, the following closed-form solution exists for the response of an end-bearing pile (Novak, 1974; Pender, 1993; Mylonakis, 1995)

$$w(z,\omega) \;=\; \frac{P}{E_p\,A_p\,\lambda}\,(\cosh\lambda z\,\tanh\lambda L \;-\; \sinh\lambda z) \tag{30}$$

where $\lambda = \sqrt{(k^* - \omega^2 \tilde{m}_p)/(E_p\,A_p)}$ is a complex wavenumber associated with the attenuation of pile response with depth. Setting the response at the pile head in equations (23) and (30) to be equal, the following implicit solution for k^* is obtained

$$\frac{\tanh L\sqrt{\dfrac{k^* - \omega^2\,\tilde{m}_p}{E_p\,A_p}}}{L\sqrt{\dfrac{k^* - \omega^2\,\tilde{m}_p}{E_p\,A_p}}} \;=\; (1+\nu_p)\left(\frac{L}{d}\right)^{-2} \sum_{m=1}^{\infty} \frac{K_0(s_m)}{K_0(s_m)\,X_{1m} \;+\; X_{2m}\,K_1(s_m)} \tag{31}$$

which can be solved in an iterative manner for k and β once the value on the right hand side is established.

For an infinitely-long pile, setting $\tanh(\lambda L) = 1$ in equation (30) and using equation (17), the following explicit solution is obtained

$$k^* \;=\; \omega^2\,\tilde{m}_p \;+\; \frac{\pi^4\,E_p}{16(1+\nu_p)^2\,A_p}\left\{\int_0^{\infty} \frac{K_0(s)}{K_0(s)\,X_1 \;+\; X_2\,K_1(s)}\;\;d\alpha\right\}^{-2} \tag{32}$$

Equations (31) and (32) are extensions of the static counterparts in Mylonakis (2001a).

Results obtained from the above averaging procedures are plotted in Figs 11 and 12. Soil impedances are depicted in Fig. 11. For infinitely-long piles, both stiffness and damping coefficients increase with frequency. Higher values of material damping result in lower Winkler stiffnesses and higher damping (Figs 11(a) and 11(c)). For piles of finite length the behaviour is more complex due to the existence of a sequence of resonant frequencies in compression extension. These frequencies can be well approximated by the expression

$$a_{res,m} = \frac{\pi}{2}\left(\frac{L}{d}\right)^{-1}\eta_s\,(2m-1) \tag{33}$$

where η_s is given by equation (4). The first resonance obtained from the above equation for $m=1$ is the cutoff frequency, a_{cutoff}, which is inherently associated with the emergence of propagating waves in the medium. For frequencies below cutoff ($0 \le a_0 \le a_{cutoff}$), stiffness is insensitive to material damping and damping coefficient is practically equal to β_s. Near cutoff frequency, stiffness drops dramatically (reaching zero for an undamped medium), and damping exhibits a jump due to the emergence of wave radiation. Beyond cutoff frequency, the behaviour resembles that of an infinitely-long pile.

To explore the role of cutoff frequency on average dynamic Winkler moduli, Fig. 12 presents results for well separated values of E_p/E_s and L/d, plotted as functions of a_0 and a_0/a_{cutoff}. Several trends are worthy of note: for frequencies below cutoff, the real part of Winkler modulus decreases monotonically with frequency. Over the same frequency range, the imaginary part is independent of frequency and practically equal to material damping. Beyond cutoff, waves start to propagate in the medium resulting in a sudden increase in damping.

As shown in Fig. 12(b), for dimensionless frequencies a_0 above approximately 0.5 the stiffness of Winkler springs becomes insensitive to soil thickness L. This is an anticipated behaviour since the waves emitted from the periphery of the oscillating pile tend to spread out in a horizontal manner without regard for the vertical dimension (Gazetas & Makris, 1991; Mylonakis, 2001b).

The above graphical representations of Winkler impedances suggest that: (1) spring and damping below cutoff are best represented in the form k/k_{static} and β as functions of a_0/a_{cutoff} (Figs 12(c) and 12(e)); (2) beyond cutoff, these parameters are best represented in the form k/G_s and β as functions of a_0 (Figs 12(b) and 12(f)), yet may require a different representation of frequency near cutoff.

Simple Representation of Winkler Stiffness and Damping

With reference to applications, simple relations for dynamic Winkler moduli were developed based on the analytical integration scheme proposed by Mylonakis (2001b), which were simplified by the authors and extended in the dynamic regime.

For frequencies below cutoff ($0 \le a_0 \le a_{cutoff}$), the following analytical formula was derived to approximate the variation of dynamic Winkler moduli with frequency

$$\frac{k}{k_{st}} = \mathrm{Re}\left[\frac{2\pi(1+2i\beta_s)}{\ln\left(\frac{2}{s}\right)-\gamma}\right] + (a_0^2 - a_{cutoff}^2) \qquad (34)(34a)$$

$$\beta = \beta_s \qquad (34b)$$

where $s = 1/2\sqrt{a_{cutoff}^2 - a_0^2/(1+2i\beta_s)}$, $\gamma\,(\simeq 0.577)$ is Euler's number; $a_{cutoff} = \pi/2\,(L/d)^{-1}\eta_s$, the last parameter being the compressibility factor in equation (4). Static stiffness k_{st} can be well approximated by the semi-analytical formula:

$$\frac{k_{st}}{G_s} \simeq \frac{2\pi}{\ln\left(\frac{4}{s_{st}}\right)-\gamma} - s_{st}^2 \quad , \quad s_{st} = \eta_s \frac{\pi}{2}\left(\frac{L}{d}\right)^{-1} \qquad (35)$$

which provides an alternative to equation (27) in Mylonakis (2001a).

For frequencies above cutoff ($a_0 > a_{cutoff}$), the corresponding expression is

$$\frac{k^*}{G_s} = \frac{2\pi(1+2i\beta_s)}{\ln\left(\frac{2}{s}\right)-\gamma} + (a_0^2 - a_{cutoff}^2)\,(1+i/2) \qquad (36)$$

The successful normalization of spring stiffness by k_{st} and G_s in equations (34a) and (35) conform to the observations in Figs 11 and 12, respectively. The above expressions are

presented graphically in Figs 13 and 14. The agreement between the approximate formulas and the numerical results cannot be overstated. Worth mentioning is the replacement of a_0 by $(a_0^2 - a_{cutoff}^2)^{1/2}$ in representing both stiffness and damping beyond cutoff, as evident in Fig. 14. It should be noticed that the two frequency variables are equivalent at high frequencies. To avoid the difficulties associated with evaluating the complex arithmetic in equations (34a) and (36), real-valued expressions are provided in Appendix.

Conclusions

Dynamic pile-soil interaction was analytically investigated through an approximate elastodynamic model by combining the concepts of a continuum and a Winkler medium. The proposed model yields solutions for the complex-valued shear tractions along axially-loaded end-bearing piles resting on rigid rock, embedded in a homogeneous viscoelastic soil stratum. Rigorous numerical solutions from the literature were employed to validate the predictions of the analytical model.

The main conclusions of the study are:

1. The model has sufficient predictive power and yet does not involve empirical constants. It compares well with rigorous numerical solutions for a wide range of frequencies, pile lengths and pile-soil stiffness ratios.
2. Dynamic Winkler modulus is, like its static counterpart, depth-dependent even in homogeneous soil (equations (26), (27)). It varies between 0.5 – 3 G_s depending on frequency, damping, slenderness and pile-soil stiffness contrast.
3. A boundary- layer phenomenon in shear tractions at the pile-soil interface is observed close to the pile head, which is attributed to the counteracting requirements for zero and maximum side resistance near the soil surface. This effect, however, appears to be of limited practical significance.
4. Pile-soil interaction is mainly governed by wave propagation in the soil, not in the pile. Accordingly, the observed wavelengths in the variation of k values along the pile in Figs

8(c) and 9(c) do not depend on pile-soil stiffness contrast (equation (28)).

5. In the high frequency range, storage stiffness of Winkler springs is independent of pile slenderness as wave propagation becomes gradually two dimensional. For the pile-soil configurations examined in this study, all impedance curves converge for dimensionless frequencies above approximately 0.5 (Fig. 12(b)).
6. The asymptotic equations derived by Mylonakis (2001b) for static Winker modulus were extended to account for dynamic stiffness and damping above and below cutoff (equations (34) and (36)). These expressions provide good approximations of dynamic Winkler impedances (Figs 13 and 14).
7. It was discovered that the Winkler spring stiffness below cutoff is best normalized by the corresponding static stiffness k_{st} as function of dimensionless frequency ratio a_0/a_{cutoff} (or ω/ω_1) (Fig. 13). On the other hand, beyond cutoff frequency, dynamic Winkler stiffness is best normalized by soil shear modulus G_s, expressed as function of incremental frequency $(a_0^2-a_{cutoff}^2)^{1/2}$ (Fig. 14). These properties stem from the dependence of the solution on the fundamental resonant frequency near cutoff, and the gradual transformation of the wave-field from three-dimensional to two-dimensional with increasing frequency beyond resonance.

As a final remark, it is fair to mention that the proposed model is limited by the assumption of linearity in soil and the pile material, as well as perfect bonding at the pile-soil interface. Exploring these effects lies beyond the scope of this paper.

Acknowledgements

The research proposed in this paper was supported by the University of Patras through a Caratheodory Grant (#*C*.580). The authors are grateful for this support. The authors would like to thank the anonymous reviewers whose comments improved the quality of the original manuscript.

References

Akiyoshi, G. (1982). Soil-pile interaction in vertical vibration induced through a frictional interface. *Earthquake Engng & Struct. Dyn* **10**, 135 – 148.

Anoyatis, G. (2009). *Elastodynamic analysis of piles for inertial and kinematic loading*. MSc Thesis, University of Patras, Rion, Greece (in Greek).

Baguelin, F. & Frank, R. (1979). Theoretical studies of piles using the finite element method. *Proc. Conf. Num. Meth. in Offshore Piling*, London, Inst. Civ. Engrs, No. **11**, 83 – 91.

Banerjee, P. K. & Sen, R. (1987). *Dynamic behaviour of axially and laterally loaded piles and pile groups*. Dynamic behaviour of foundations and buried Structures (Developments in Soil Mechanics and Foundation Engineering, Vol. 3) (Eds. P. K. Banerjee and R. Butterfield), Elsevier Applied Science, London, 1987, 95 – 133.

Baranov, V. A. (1967). On the calculation of an embedded foundation (in Russian), *Vorposy Dinamiki i Prognostic*. Polytechnical Institute of Riga, Latvia, No. 14, 195 – 209.

Bhattacharya, S., Madabhushi, S. P. G. & Bolton, M. D. (2004). An alternative mechanism of pile failure in liquefiable deposits during earthquakes. *Géotechnique* **54**, No. 3, 203 – 213.

Blaney, G. W., Muster, G. L. & O'Neil, M. W. (1987). Vertical vibration test of a full-scale pile group. ASCE, *Geotech. Special Publ*., No. 11, 149 – 165.

Blaney, G. W., Kausel, E. & Roesset, J. M. (1976). Dynamic stiffness of piles. *Proc 2nd Int. Conf, Num. Methods Geomech*, Blacksburg, 1001 – 1012.

Boulanger, R. W., Curras, C. J., Kutter, B. L., Wilson. D. W. & Abghari, A. (1999). Seismic-pile-structure interaction experiments and analyses. *J. Geotech. Engng* **125**, No. 9, 750 – 759.

El-Marsafawi, H., Han, Y. C. & Novak, M. (1992). Dynamic Experiments on Two Pile Groups. *J. Geotech. Engng., ASCE*, Vol. **118**, No. 6, 839 – 855.

El-Sharnouby, B. & Novak, M. (1990). Stiffness constants and interaction factors for vertical response of pile groups. *Can. Geotech. J.* **27**, 813 – 822.

El-Naggar, M. H. (2000). Vertical and torsional soil reactions for radially inhomogeneous soil layer. *Structural Engng & Mechanics* **10**, No. 4, 299 – 312.

Gazetas, G. & Makris, N. (1991). Dynamic pile-soil-pile interaction. Part I: Analysis of axial vibration. *Earthquake Engng & Struct. Dyn* **20**, 115 – 132.

Graff, K. F. (1975). *Wave motion in elastic solids*. Oxford University Press. London.

Guo, W. D. (2000). Vertically loaded single piles in Gibson soil. *J. Geotech. & Geoenviron. Engng*, ASCE **126**, No. 2, 189 – 193.

Ji, F. & Pak, R. Y. S. (1996). Scattering of vertically-incident P-waves by an embedded pile. *Soil Dyn. Earthquake Engng* **15**, No. 3, 211 – 222.

Kaynia, A. M. & Kausel, E. (1982). Dynamic stiffness and seismic response of pile groups. *Research Rep. R82-03*, Massachusetts Inst. of Technology.

Knappett, J. A. & Madabhushi S. P. G. (2009). Influence of axial load on lateral pile response in liquefiable soils. Part I: physical modelling. *Géotechnique* **59**, No. 7, 571 – 581.

Mylonakis, G. (1995). *Contributions to static and seismic analysis of piles and pile-supported bridge piers*. Ph.D. Thesis, State University of New York at Buffalo.

Mylonakis, G. (2001a). Winkler modulus for axially loaded piles. *Géotechnique* **51**, No. 5, 455 – 461.

Mylonakis, G. (2001b). Elastodynamic model for large-diameter end-bearing shafts. *Soils & Foundations* **41**, No. 3, 31 – 44.

Nogami, T. & Novak, M. (1976). Soil-pile interaction in vertical vibration. *Earthquake Engng & Struct. Dyn* **4**, 277 – 293.

Novak, M. (1974). Dynamic stiffness and damping of piles. *Can. Geotech. J.* **11**, No. 4, 574 – 598.

Novak, M., Nogami, T. & Aboul-Ella, F. (1978). Dynamic soil reactions for plane strain case. *J. Engng Mech. Div.*, ASCE **104**, No. 44, 953 – 959.

Novak, M. (1991). Piles under dynamic loads: State of the art. Proc. *2nd Int. Conf. on Recent Advances in Geotech. Earthquake Engng and Soil Dynamics*, St. Louis, 2433 – 2456.

O'Rourke, M. J. & Dobry, R. (1978). Spring and dashpot coefficients for machine foundations on piles. *Publ. SP-10, American Concrete Institute*, Detroit, 177 – 198.

Pak, R. Y. S. & Ji, F. (1993). Rational mechanics of pile-soil interaction. *J. Engng. Mech.*, ASCE **119**, No. 4, 813 – 832.

Pender, M. J. (1993). Aseismic pile foundation design analysis. *Bulletin NZ National Society for Earthquake Engng* **26**(1), 49 – 160.

Poulos, H. G. & Davis, E. (1980). *Pile Foundation Analysis and Design*. Wiley, New York.

Rajapakse, R. K. N. D. (1990). Response of an axially loaded elastic pile in a Gibson soil. *Géotechnique* **40**, No. 2, 237 – 249.

Randolph, M. F. & Wroth, C. P. (1978). Analysis of deformation of vertically loaded piles. *J. Geotech. Engng*, ASCE **104**, No. 12, 1465 – 1488.

Roesset, J. M. (1980). Stiffness and damping coefficients of foundations, O'Neil, Dobry, Editors, *Dyn. Resp. Pile Fdns,* ASCE, 1 – 30.

Reese, L. C. & Van Impe, W. F. (2000). *Single piles and pile groups under lateral loading*. Balkema Publ, Rotterdam, Netherlands.

Saitoh, M. (2005). Fixed-head pile bending by kinematic interaction and criteria for its minimization at optimal pile radius. *J. Geotech. & Geoenviron. Engng*, ASCE **131**, No. 10, 1243 – 1251.

Sanchez-Salinero, I. (1982). Static and dynamic stiffness of single piles. *Geotech Engng Rep*. GR82-31, Austin: University of Texas.

Scott, R. F. (1981). *Foundation analysis*. Prentice Hall.

Seo, H., Basu, D., Prezzi, M. & Salgado, R. (2009). Load-settlement response of rectangular and circular piles in multilayered soil. *J. Geotech. & Geoenviron. Engng*, ASCE **135**, No. 3, 420 – 430.

Syngros, K. (2004). *Seismic response of piles and pile-supported bridge piers evaluated through case histories*. Ph.D. Thesis, City University of New York.

Tajimi, H. (1969). Dynamic analysis of a structure embedded in an elastic stratum. *Proceedings 4th WCEE*, Chile.

Tazoh, T., Shimizu, K., Wakahara, T. (1987). Seismic observations and analysis of grouped piles. Dynamic Response of Pile Foundations: experiment, analysis and observation, *Geotech. Special Publ*., ASCE, No. 11, 1 – 20.

Veletsos, A. S. & Dotson, K. W. (1986).Impedances of soil layer with disturbed boundary zone. *J. Geotech. Engng*, ASCE **112**, No. 3, 363 – 368.

Wolf, J. P., Meek, J. W. & Song, C. (1992). Cone models for a pile foundation, Piles Under Dynamic Loads, *Geotech. Special Publ*., ASCE, No. 34, 94 – 113.

Appendix

Equations (34) and (36) can be cast in the real-valued form by the expressions:

(a) Below cutoff $(0 \le a_0 \le a_{cutoff})$:

$$\frac{k}{k_{st}} = 4\pi \frac{X - 2\beta_s Y}{X^2 + Y^2} + (a_0^2 - a_{cutoff}^2) \tag{A-1a}$$

$$\beta = \beta_s \tag{A-1b}$$

(b) Above cutoff $(a_0 > a_{cutoff})$:

$$\frac{k}{G_s} = 4\pi \frac{X - 2\beta_s Y}{X^2 + Y^2} + (a_0^2 - a_{cutoff}^2) \tag{A-2a}$$

$$\beta = 4\pi \frac{Y + 2\beta_s X}{X^2 + Y^2} + \frac{1}{2}(a_0^2 - a_{cutoff}^2) \tag{A-2b}$$

where

$$X = 4\ln 2 - 2\gamma + \ln(1 + 4\beta_s^2) - \ln(\sqrt{a^2 + b^2}) \tag{A-3}$$

$$Y = 2 \arctan\left(\frac{b}{\sqrt{a^2 + b^2} + a}\right) \tag{A-4}$$

$$a = (1 + 4\beta_s^2)\, a_{cutoff}^2 - a_{0,}^2 \qquad b = 2\beta_s a_0^2 \tag{A-5a,b}$$

List of Captions

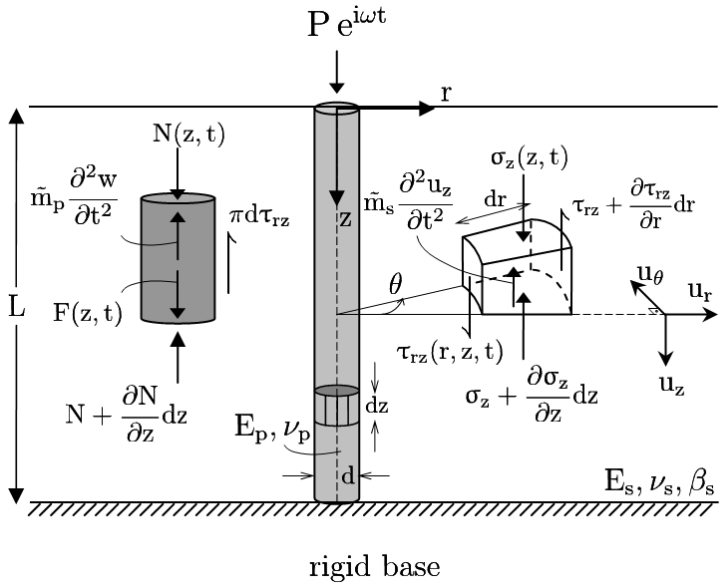

Figure 1. System considered: main parameters and notation

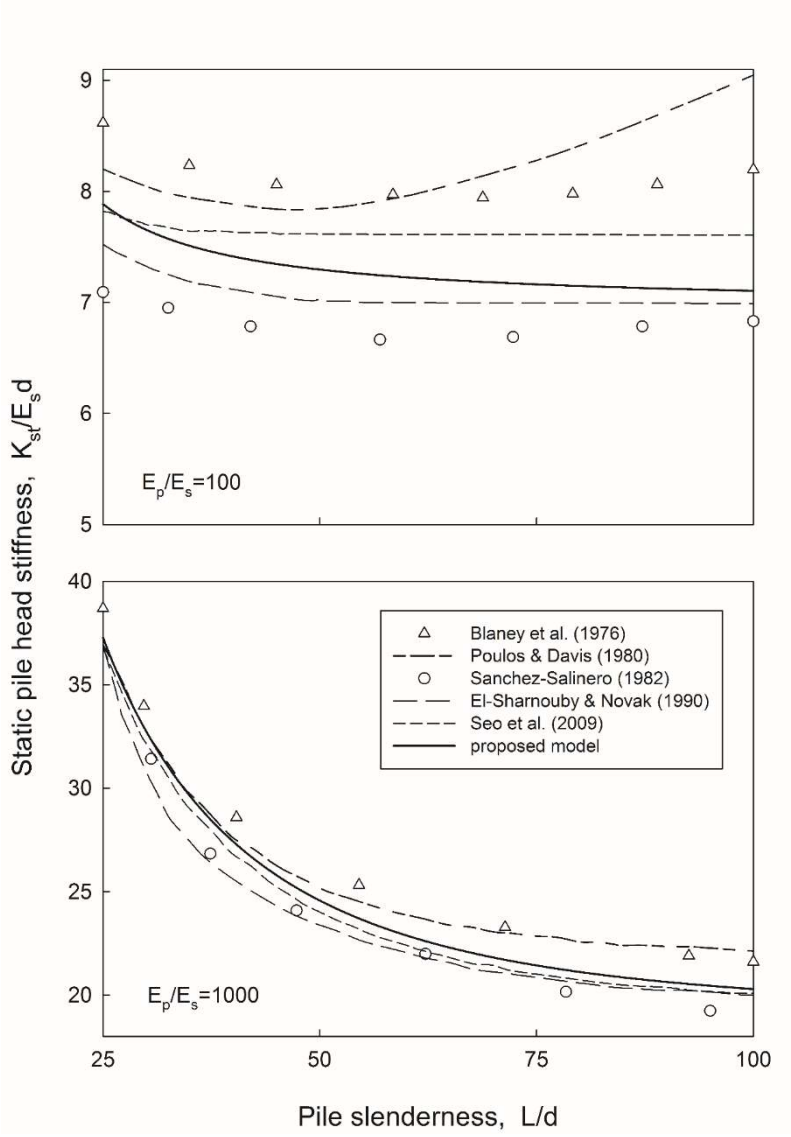

Figure 2. Static pile head stiffness of end-bearing piles. Comparison of the proposed analytical model with results from published numerical solutions

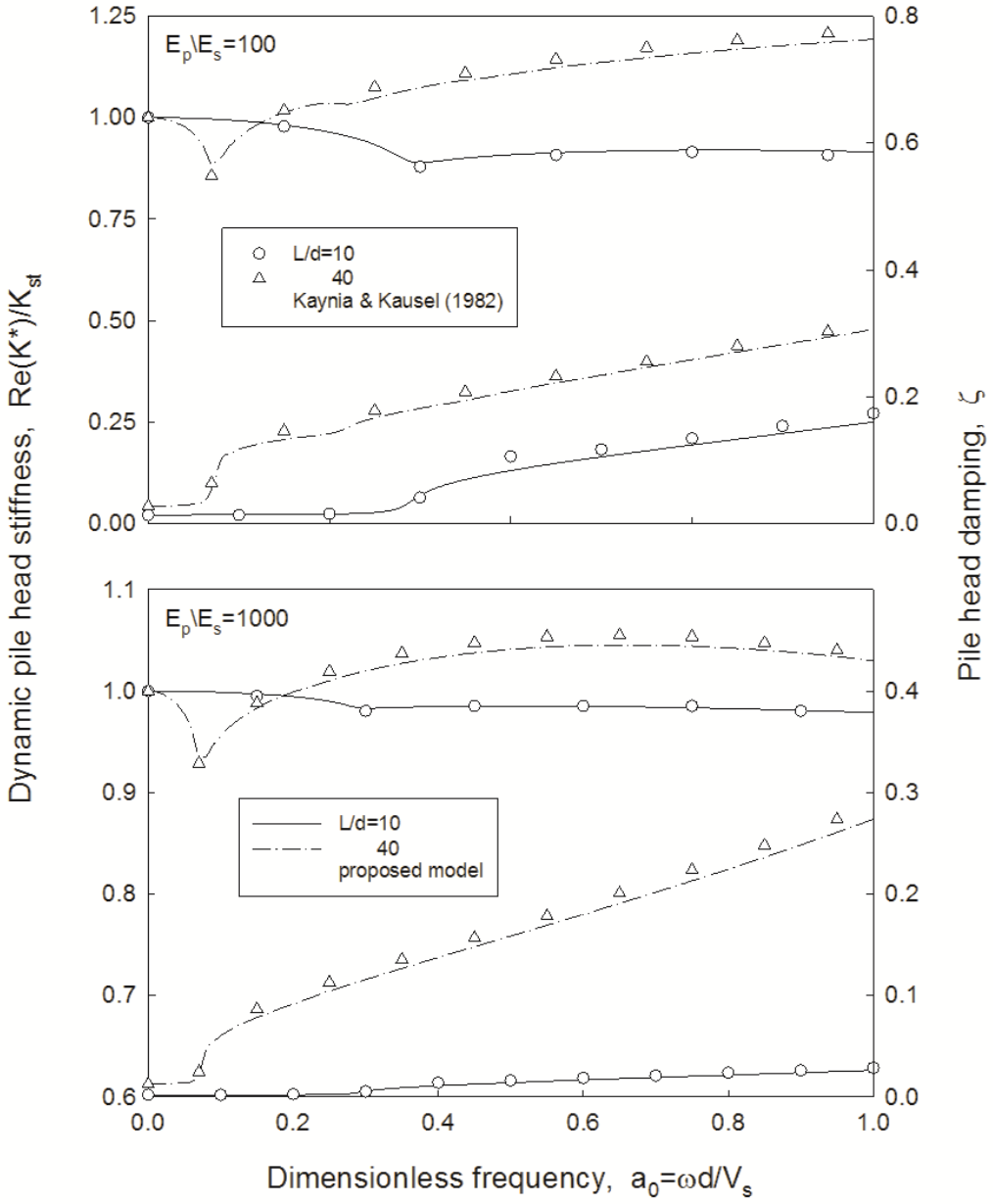

Figure 3. Comparison of dynamic pile head stiffness and damping obtained with the proposed analytical model and from the rigorous solution of Kaynia & Kausel (1982); $\beta_s = 0.05$

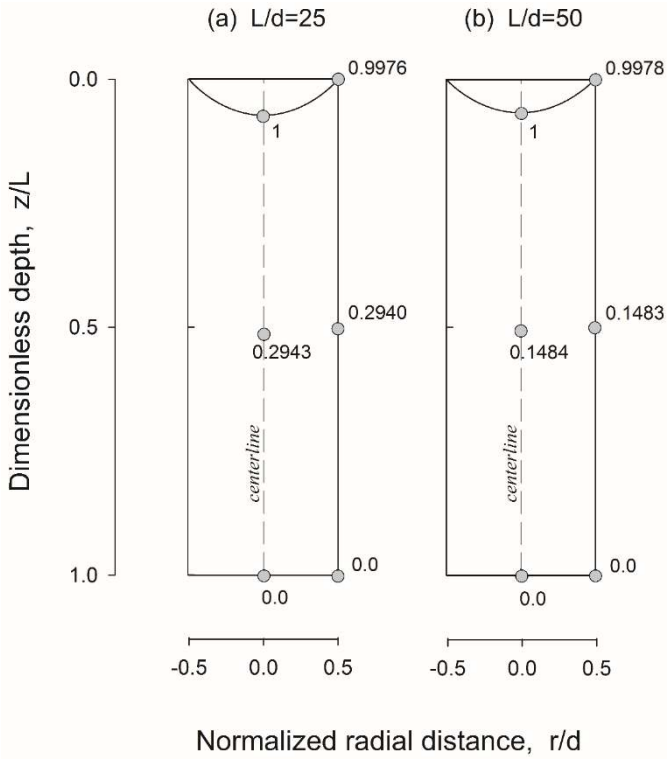

Figure 4. Variation of vertical displacement within the pile cross section at three elevations, for two end-bearing piles. Results are normalized with respect to pile head settlement at the centerline; $E_p/E_s = 100$, $\nu_p = 0.2$

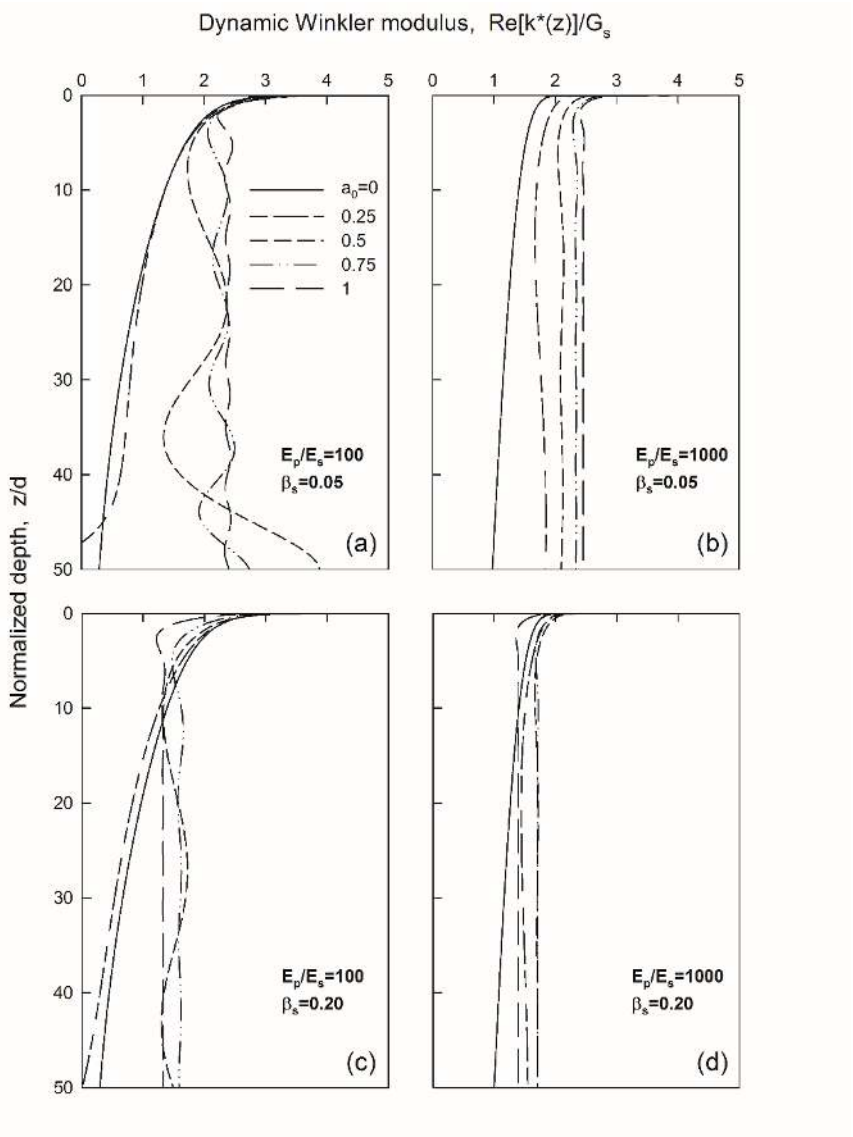

Figure 5. Variation with depth of dynamic Winkler spring modulus for an infinitely long pile

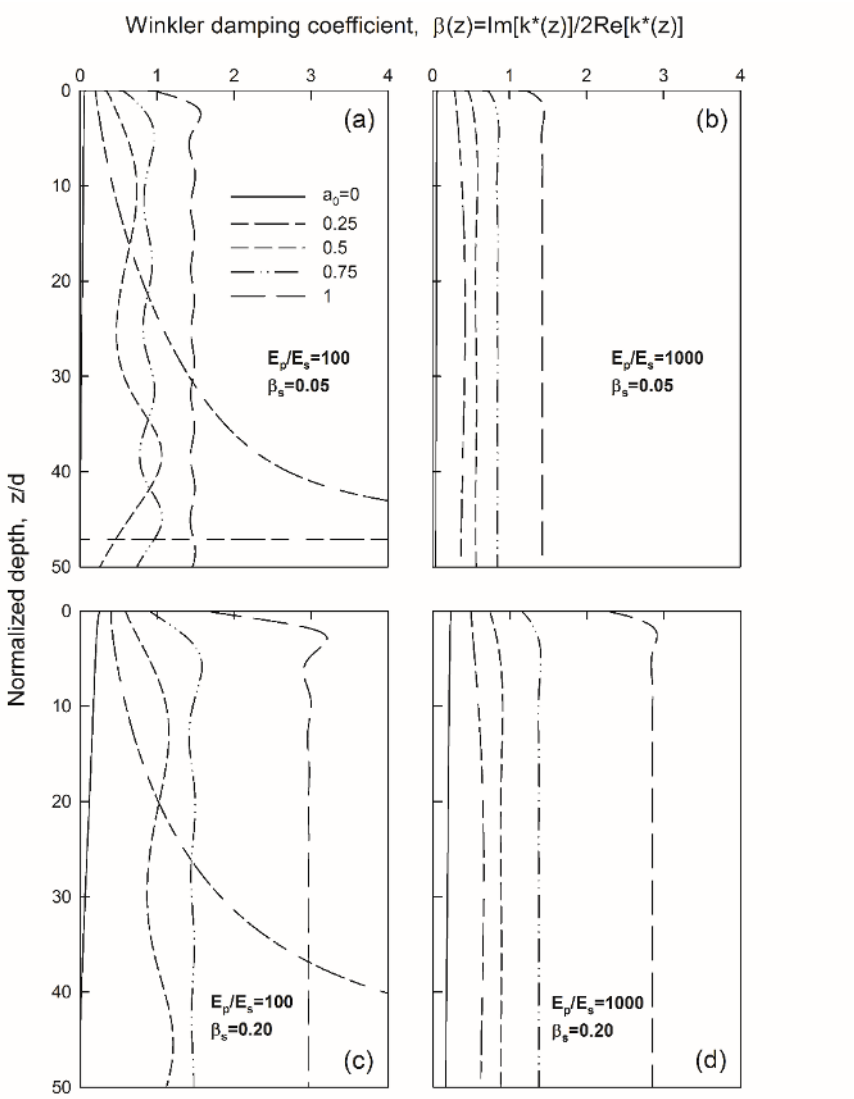

Figure 6. Variation with depth of Winkler damping coefficient for an infinitely long pile

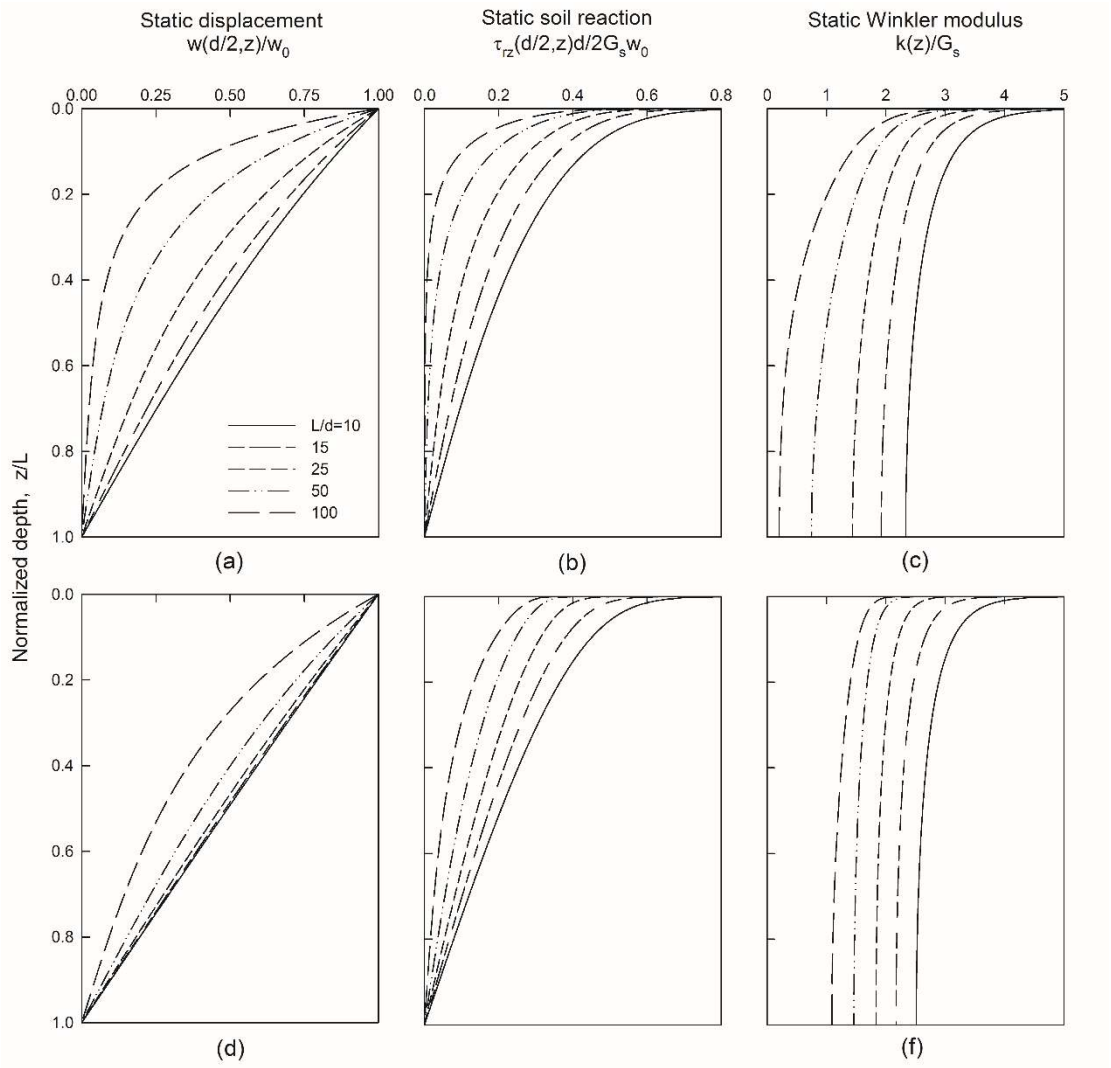

Figure 7. Variation with depth of static displacement, soil reaction and Winkler spring modulus for end-bearing piles of different slenderness L/d; $E_p/E_s = 100$ (a to c), $E_p/E_s = 1000$ (d to f)

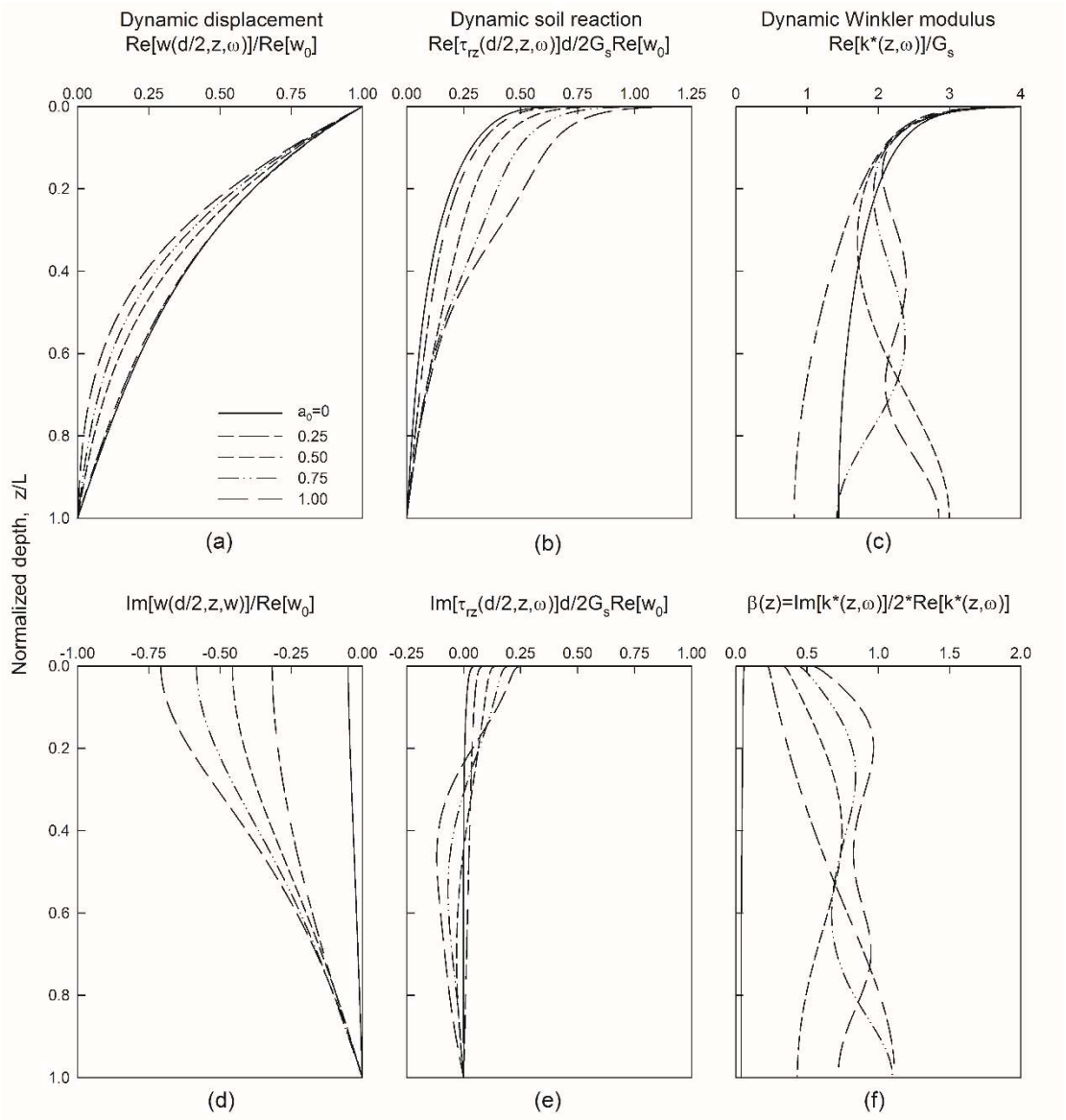

Figure 8. Variation with depth of dynamic displacement, soil reaction and Winkler moduli for end-bearing piles; $\beta_s = 0.05$, $E_p/E_s = 100$

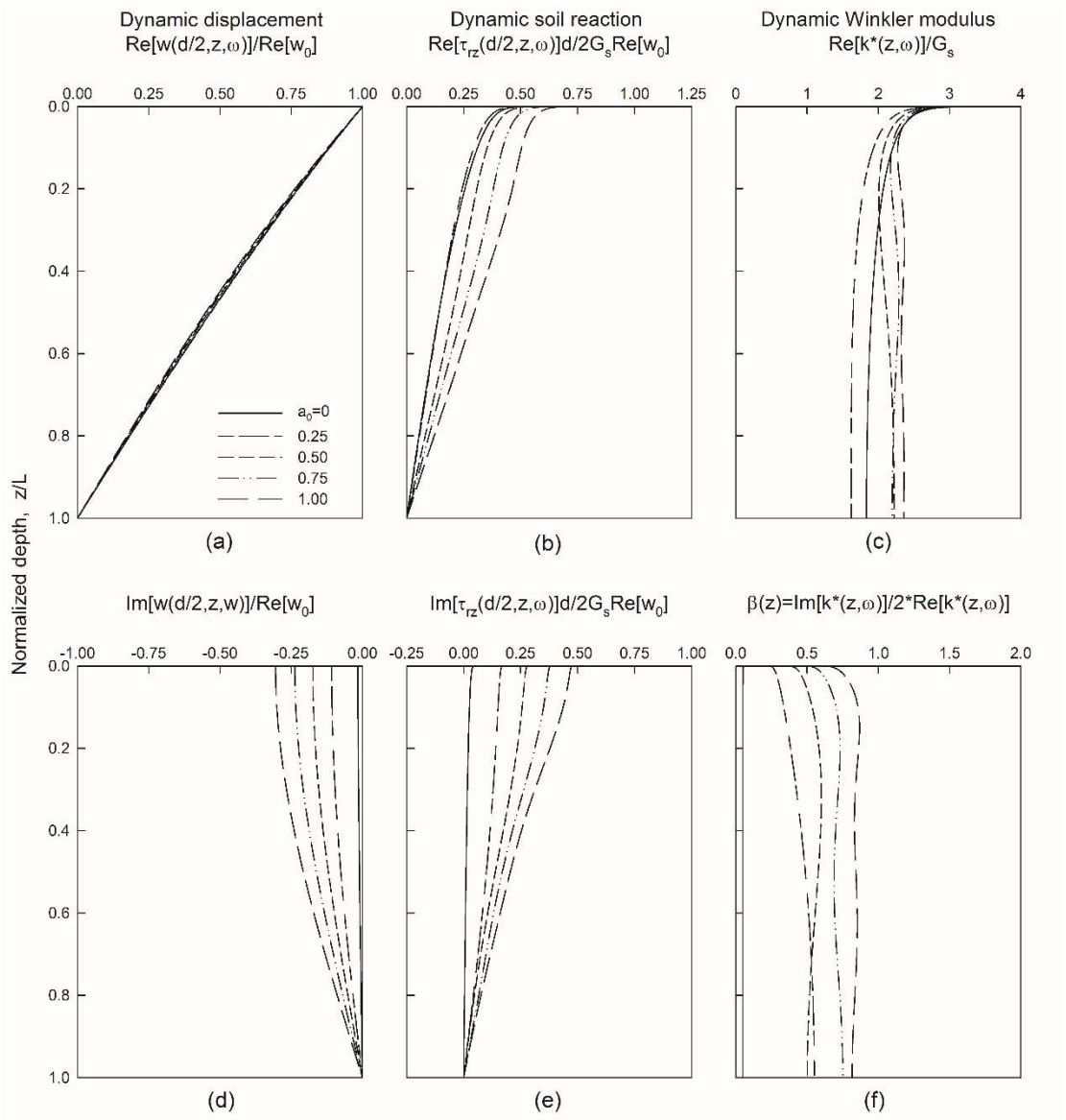

Figure 9. Variation with depth of dynamic displacement, soil reaction and Winkler moduli for an end-bearing; $\beta_s = 0.05$, $E_p/E_s = 1000$

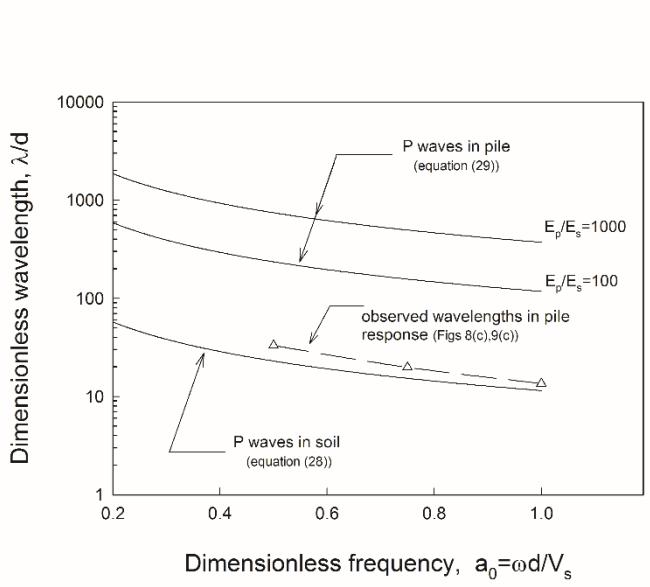

Figure 10. Dependence of P-wavelengths in pile and soil on excitation frequency for different pile-soil stiffness ratio

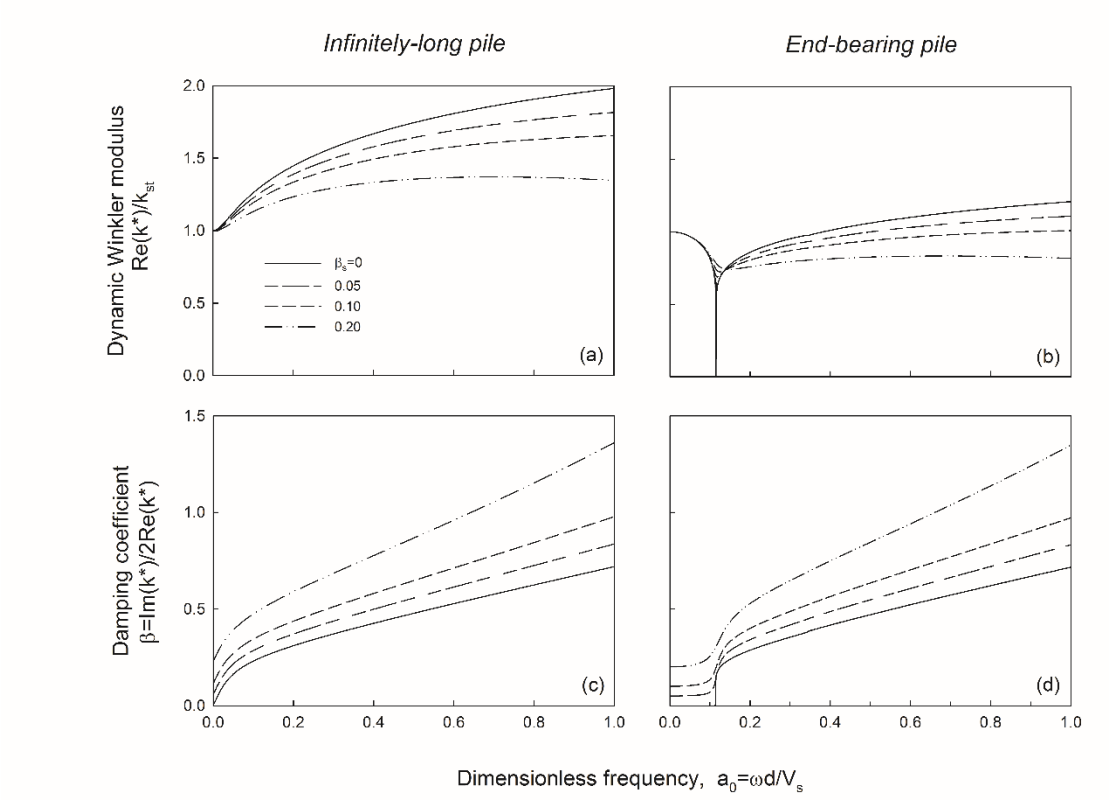

Figure 11. Effect of soil material damping on average dynamic Winkler impedances for both infinitely-long and end-bearing ($L/d = 25$) pile; $E_p/E_s = 1000$

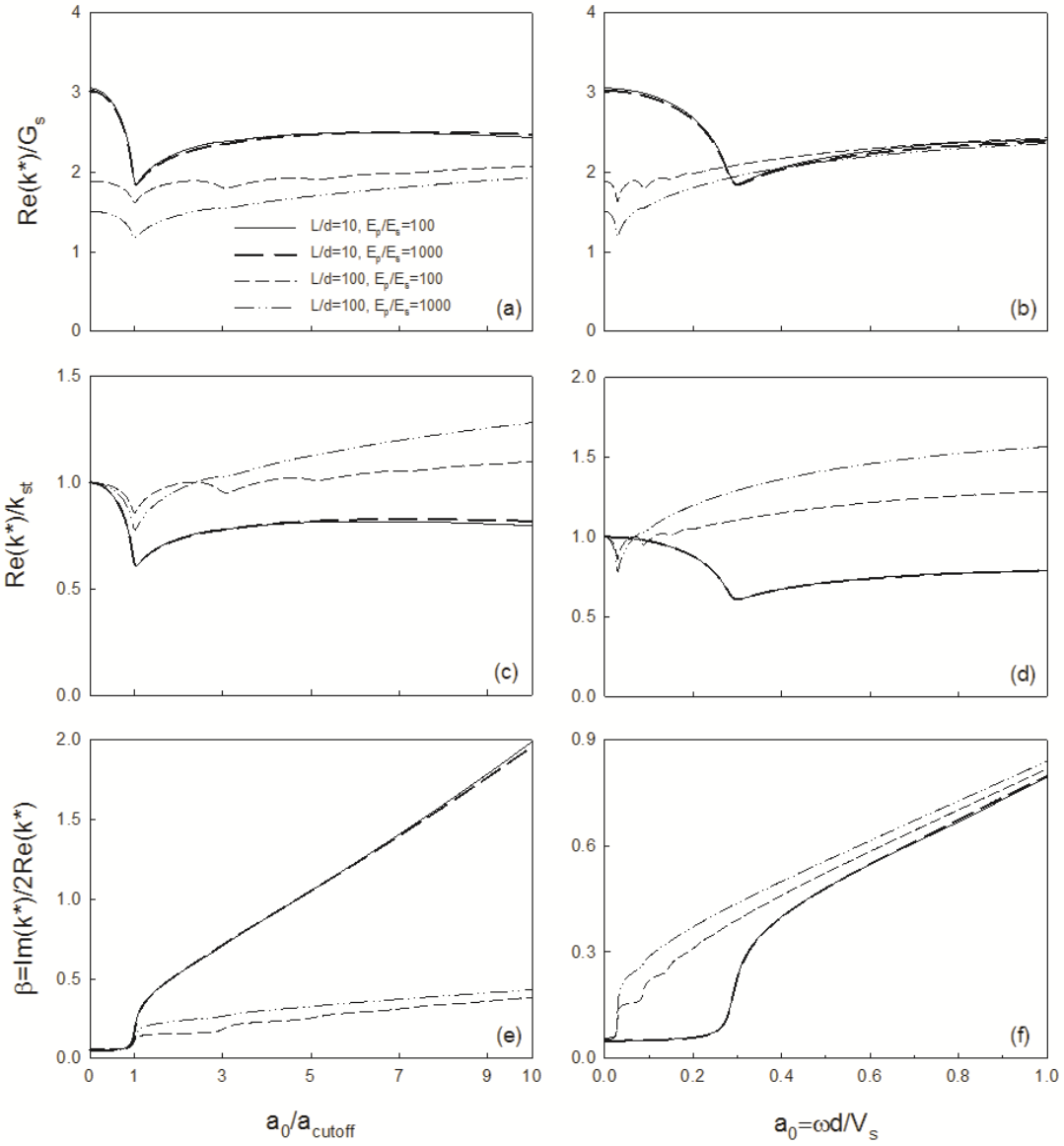

Figure 12. Dynamic Winkler impedance coefficients for end-bearing piles of different slenderness $\mathrm{L/d}$ and pile-soil stiffness $\mathrm{E_p/E_s}$; $\beta_s = 0.05$

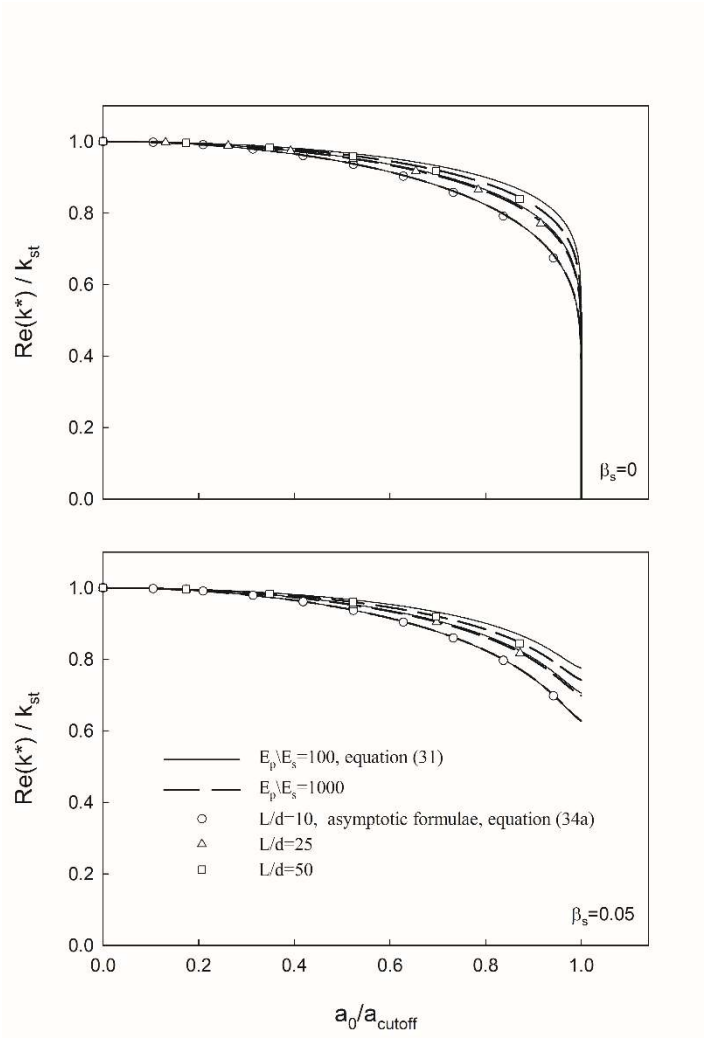

Figure 13. Depth-independent Winkler modulus for end-bearing piles. Comparison of the rigorous analytical solution with the approximate expression in equation (34a)

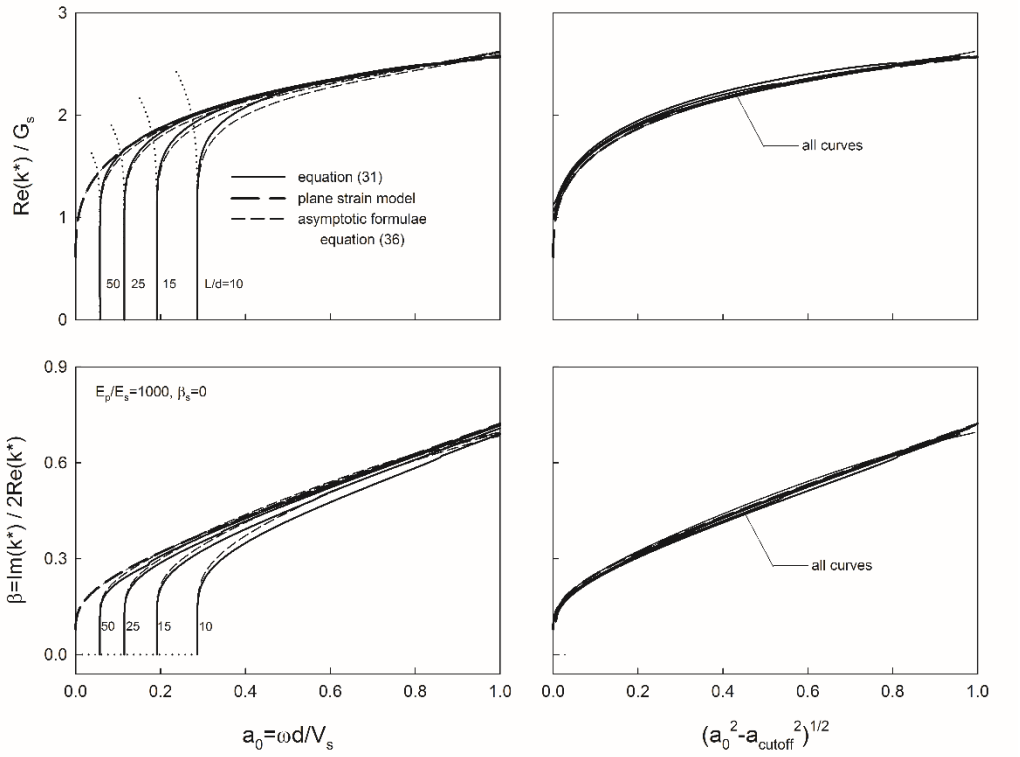

Figure 14. Depth-independent Winkler moduli for end-bearing piles. Comparison of the rigorous analytical solution with the approximate expression in equation (36) using two different representations of frequency [In the plane strain model, $a_{cutoff} = 0$]